ADVANCED OPTICAL MATERIALS
www.advopticalmat.de

Full-Color Luminescence from Single-Component Hydrocarbon Crystal: RGB Emission by Altering Molecular Packing Under Pressure

Takeshi Nakagawa, Songhao Guo, Martina Vrankić, Philip Dalladay-Simpson, Kejun Bu, Dong Wang, Xia Yin, Ke Liu, Hongshan Deng, Jianbo Zhang, Chunsheng Xia, Yonggang Wang, Xujie Lü, Ho-kwang Mao, and Yang Ding**

Full-color emission from solid single-component organic materials is highly desired to realize inexpensive and non-toxic organic electronics. However, as the three primary colors, red, green, and blue (RGB), have significantly different energies, observation of RGB luminescence from a single-component molecule is extremely challenging. In this study, a coronene nanorod single-component single-crystal is prepared, which exhibits blue fluorescence at ambient conditions and realizes full-color emission, for the first time, by altering the molecular packing through high-pressure compression. A valuable insight into the relationships between structure and optical properties of coronene at high pressures is obtained by combining various spectroscopic studies. During compression, it is found that the tuneable piezochromic luminescence of coronene is strictly related to the molecular packing and crystallographic symmetry. This study not only provides insight into the structure-optical property relationships of hydrocarbon but also promotes the development of single molecular systems with different molecular packing that exhibit RGB emissions even at ambient conditions even with a single excitation wavelength.

1. Introduction

Solid-state organic luminescent materials with tuneable optical properties have gained increasing research importance owing to the recent high demand for organic optoelectronic and photonic applications, organic semiconductors, and nanoelectronics.[1–3] To achieve full-color emission, or even emission of the three primary colors: red, green, and blue (RGB), from a single-component organic material in the solid-state is a major challenge. There are various ways to generate RGB luminescence from single-component systems, for example, changing the excitation energy,[4] altering auxochromes (color helpers) in organic dyes,[5] or changing the environment between polymer matrix, solution, and crystals.[6] However, to date, no single-component organic system in a single crystal form that exhibits RGB without changing the excitation energy has been reported.

The optical properties of organic molecules depend crucially and closely on their molecular structures and packing in the crystal, crystal morphology, phase, and various external stimuli. The challenge for crystal engineering lies in fabricating high-quality crystals with suitable sizes and shapes and desired properties. However, growing single crystals with different optical properties without the necessary information can be a time-consuming process. Recently, the use of high pressure has proven to be an effective approach to uncovering the relationship between the crystal structure and material properties.[7] Pressurization can effectively alter the molecular packing of fluorescent materials. Through the combination of various spectroscopic techniques, we can investigate pressure-induced changes in the emission wavelength, intensity, intermolecular interaction, molecular conformation, and phase transformation. These pressure-dependent changes in the emitted color of luminescent materials are known as piezochromism, which is a direct consequence of the perturbation to the electronic bandgap energy of the electronic transition in luminescent materials.[8] Well-known piezochromic behaviors are found in van der Waals materials, such as donor–acceptor complexes, polymers, molecular systems, and liquid crystals.[9] In these materials, the molecular packing can be altered sensitively with changes in external stimuli, leading to significant changes in the optical bandgap and consequently the chromaticity of their emission.

Recently, carbon-rich organic molecular luminescent solids, such as polycyclic aromatic hydrocarbons (PAHs), have gained

T. Nakagawa, S. Guo, P. Dalladay-Simpson, K. Bu, D. Wang, X. Yin, K. Liu, H. Deng, J. Zhang, C. Xia, Y. Wang, X. Lü, H.-kwang Mao, Y. Ding
Center for High Pressure Science and Technology Advanced Research
10 Xibeiwang East Road, Haidian, Beijing 100094, P. R. China
E-mail: takeshi.nakagawa@hpstar.ac.cn; yang.ding@hpstar.ac.cn
M. Vrankić
Division of Materials Physics
Ruđer Bošković Institute
Bijenička 54, Zagreb 10000, Croatia

The ORCID identification number(s) for the author(s) of this article can be found under https://doi.org/10.1002/adom.202300586

DOI: 10.1002/adom.202300586

considerable amount of interest owing to their high degree of π-conjugated structure, which inherently exhibits excellent crystal structure tuneability.[10] In particular, coronene has a unique electronic structure owing to the delocalized pi-electrons between the six outer rings,[11] which has led to the development of several coronene-based optoelectronic materials.[12] The evidence provided by Yin and Liu shows remarkable photostability of functionalized coronenes, which is attributed to the high highest occupied molecular orbital (HOMO) energy level of the coronene core, making them potential candidates for organic devices that can be processed in solution.[13] It has been reported that PAH-based co-crystals and derivatives exhibit piezochromic properties that represent new concepts in this research area,[14] however, they often require complex organic synthesis and development of an engineering strategy for multicomponent assemblies. Furthermore, our fundamental understanding of piezochromic mechanisms remains elusive, making the development of piezochromic materials and the prediction of their behavior extremely challenging. To better understand the relationship between structure and optical properties, single-component, small-molecule systems such as coronene have an advantage over polymers or multicomponent systems because their properties can be easily characterized and they are synthetically reproducible.

Under ambient conditions, pure coronene has a monoclinic symmetry with two molecules per unit cell, space group $P2_1/n$, and lattice parameters: $a = 10.08$ Å, $b = 4.69$ Å, $c = 15.65$ Å, and $\beta = 106.0$∘, known as the conventional gamma-herringbone (γ-) polymorph.[15] Upon crystallization of the PAH coronene in the presence of a magnetic field, an enantiotropic polymorph forms in a β-herringbone motif, with a significant change of up to 35° in the nearest-neighbor herringbone angle.[16]

Due to the weakening of hydrogen bonding in the β-polymorph caused by the nearly linear CH$\cdots\pi$ hydrogen bonding and the herringbone nearest-neighbor angle of 49.71°, the optical properties of the β-herringbone structure are altered to the extent that it panchromatically absorbs from the UV to the near-IR. Despite the notable differences in packing, β- and γ-coronenes are enantiotropic polymorphs that possess the same monoclinic $P2_1/n$ crystal symmetry, and both pack with $Z = 2$ molecules per unit cell. According to recent spectroscopic and crystallographic results, pressure-triggered structural phase transitions in coronene were observed at ≈1.5 and 12.2 GPa, with the high-pressure phases exhibiting monoclinic and orthorhombic symmetries with space groups $P2/m$ and $Pmmm$, respectively.[17] However, there are studies that point to a completely different structural arrangement of the non-ambient phase. Zhao and Chanyshev found that Yamamoto's claim that the orthorhombic assembly already exists at a relatively low pressure of 1.1 GPa is not true.[18] Undoubtedly, there are still considerable uncertainties in identifying coronene polymorphs and deciphering their precise structural arrangement at high-pressure. For example, Chanyshev suggested that a large deviation (up to −0.15°) of peak [010] in the high-pressure patterns of coronene might indicate an error in the selection of the $P2/m$ space group for the high-pressure phase above 2.9 GPa, however, he failed to provide adequate evidence for this finding. Therefore, complementary high-precision indexing methods are crucial for the reconstruction of 3D elementary monoclinic axes, which may vary considerably in length. Incorrect assumptions can be very detrimental when it comes to deriving the correct unit cell. It has been suggested that phase assignment based only on precise reproduction, provides evidence of polymorphism, independent of X-ray structure determination, through the synergy between corrected, high-precision density functional theory (DFT) calculations and lattice phonon Raman characterization.[19]

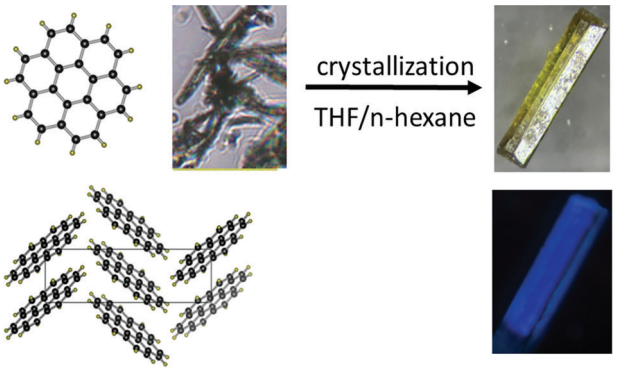

Scheme 1. Re-crystallization process of nano-needle to nano-rod single-crystal coronene through slow volatilization of the tetrahydrofuran (THF)/*n*-hexane mixture.

In this work, we combined photoluminescence (PL), UV–vis absorption, Raman and IR spectroscopic measurements, and synchrotron X-ray diffraction (XRD) experiment with diamond anvil cell (DAC) techniques to systematically investigate the piezochromic properties of pristine coronene up to 40 GPa at room temperature (RT). During compression, we observed continuous redshift in the emission band exhibiting color changes from blue to green, and finally to red. The relationship between structure and optical properties showed that the successive color changes were caused by the associated change in molecular packing in the ground state. In addition, significant emission enhancement was observed when changing from blue to green. Furthermore, all Raman, IR, and UV–vis absorption spectroscopy measurements showed that coronene underwent an irreversible chemical ring-opening reaction to an amorphous state at 27 GPa, which clarifies a number of inconsistencies reported in previous high-pressure studies of coronene.[17] Here, we demonstrated that single-component, single-crystalline coronene can exhibit RGB emission only by altering its molecular packing. This makes coronene the most promising candidate for the solid single-component organic molecule that exhibits RGB emission even under ambient conditions using single excitation energy.

2. Results and Discussion

Yellow single-crystalline coronene nano-rods were prepared by re-crystallizing nanoneedle coronene crystals in a mixture of tetrahydrofuran (THF) and *n*-hexane, as shown in **Scheme 1**. The nanorod crystals were characterized using the single-crystal XRD, Raman, and IR spectroscopy measurements, and it was confirmed that the obtained data were identical to those of the previously reported γ-polymorph coronene. Details of the crystal structure, refined XRD data, and Raman and IR spectra can be found in the Supplementary Information. (Figures S1–S4, Supporting Information).

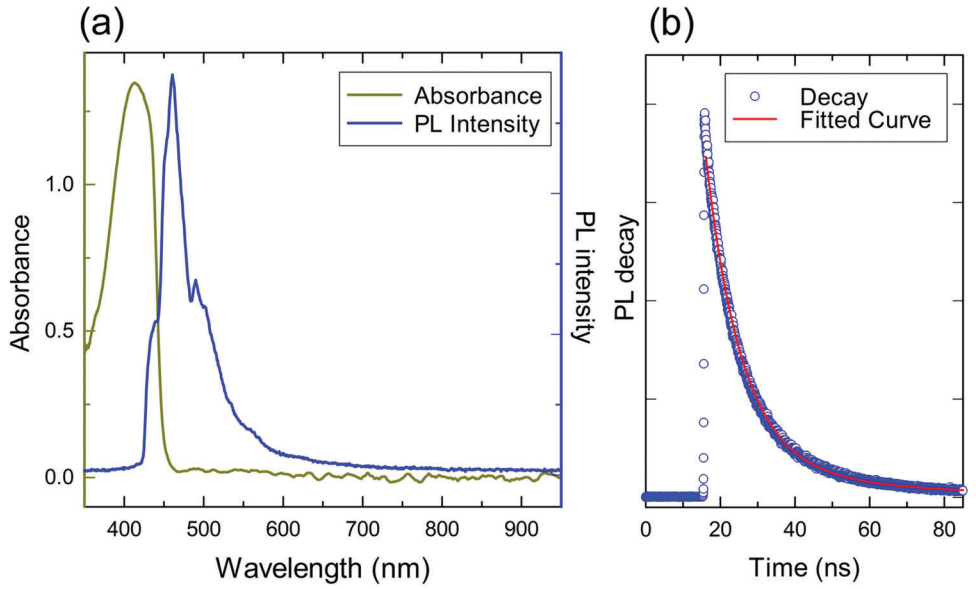

Figure 1. a) UV–vis absorption (yellow) and PL spectrum of nanorod $C_{24}H_{12}$ at 405 nm laser (blue) at ambient conditions. b) Transient decay spectrum of $C_{24}H_{12}$ obtained at ambient conditions. The red curve represents the fitted curve of the data for extracting prompt and delayed emission components.

The photoluminescent micrograph in Scheme 1 shows that the nanorod coronene exhibited blue fluorescence under UV light. In **Figure 1**, the PL spectrum of coronene at ambient conditions shows a broad emission band in the visible range between 415 and 650 nm with a maximum intensity at 459 nm (E_{em} = 2.70 eV). The observed emission band was nearly identical to the band of a self-trapped exciton (STE) luminescence exhibited by flakes of ultra-pure single-crystal coronene obtained through sublimation crystal growth.[20] The PL spectra were converted to Commission International de l'Eclairage (CIE) coordinates with (x, y) = (0.22, 0.21), which are indicated in blue in the CIE chromaticity diagram. Figure 1b shows the measured PL lifetime, where the transient decay spectra were best fitted with two components, prompt (τ_p = 9.55(4) ns and Amp_{rel} = 89.7(2)%) and delayed (τ_d = 39.6(3) ns and Amp_{rel} = 10.4(2)%). The UV–vis absorption spectrum exhibited a sharp absorption edge corresponding to the HOMO–LUMO transition[21] with maximum absorption at 412 nm. By extrapolating the linear portion of the Kubelka–Munk [F(R)] plots,[22] the optical bandgap of coronene at ambient conditions were estimated to be 2.82 eV (Figure S5, Supporting Information). The optical property of nano-rod crystalline coronene at ambient conditions can be classified as fluorescence emission and a suppressed thermally activated delayed fluorescence (TADF) under oxygen.[23]

The pressure-dependent emission spectra of the single-crystal coronene were collected up to 24 GPa with a 405 nm excitation laser. During the compression process, the position of the peak maximum of PL exhibited a continuous and significant red-shift from 459 nm (blue) to 740 nm (near-IR), a total shift of 281 nm at pressures up to 21.6 GPa (13.0 nm GPa^{-1}). The obtained spectra were converted to the calculated CIE coordinates and plotted on a 1931 CIE chromaticity diagram (**Figure 2**). The calculated chromaticity coordinates clearly demonstrate that the coronene nanorods exhibited full-color piezochromic luminescence that included three primary RGB colors. Piezochromic luminescence is commonly observed in various organic materials, especially in large planar molecules with strong $\pi-\pi$ interactions, however, it is extremely rare to observe full-color emission induced by pressure.

Figure 3 shows the selected emission spectra of coronene under pressures up to 23.0 GPa, and the extracted pressure-dependent PL maximum position and integrated PL intensity are shown in Figure 3b. A sharp increase in intensity at 0.2 GPa and a gradual decrease to 0.8 GPa was observed during the first pressurization. At 1.0 GPa, the shape of the spectrum changed significantly and the emission color changed from blue to green, with the integrated intensity increasing to the same level of 0.2 GPa. As the pressure further increased, emission intensity also

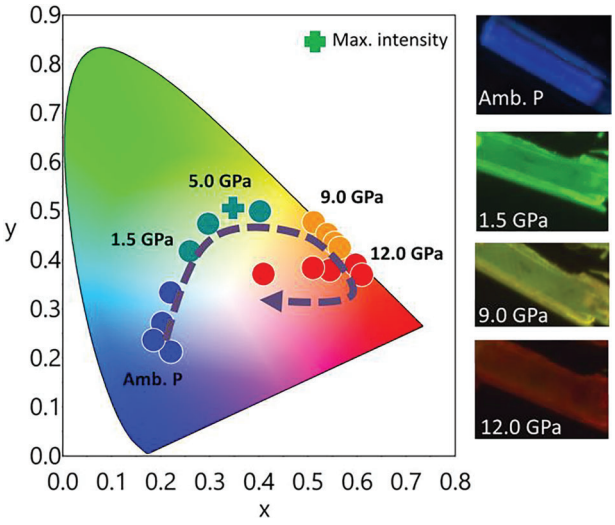

Figure 2. Chromaticity coordinates of emissions and PL micrographs obtained during compression of $C_{24}H_{12}$ with a wide range of color tuneability.

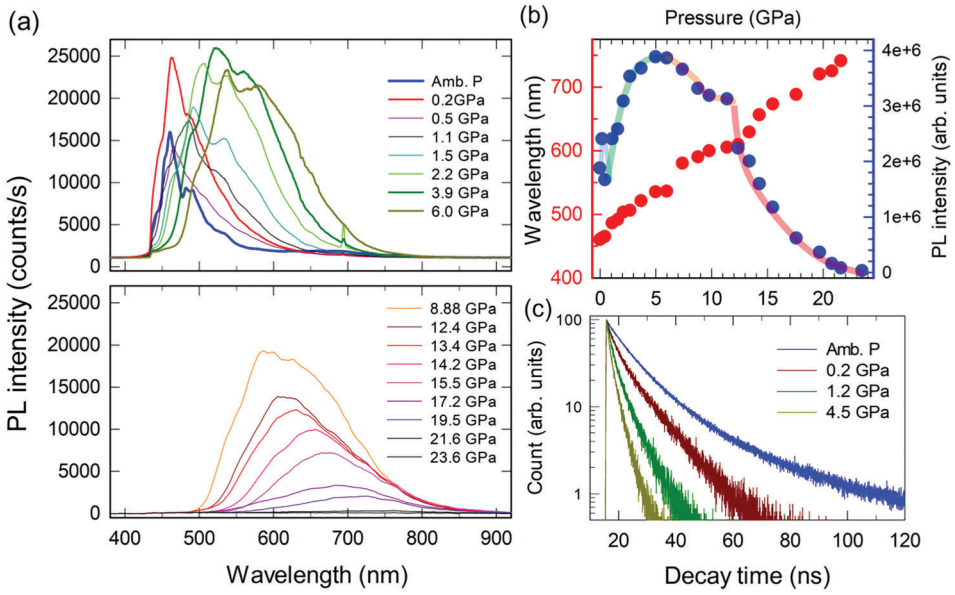

Figure 3. a) PL spectra of $C_{24}H_{12}$ at a pressure range of 0.01–23.5 GPa, excited using a 405 nm laser. Top: intensity increases up to 6.0 GPa. Bottom: intensity decreases above 8 GPa. b) Pressure-dependent emission peak maximum position (red, left axis) and integrated PL intensity (blue, right axis). The pale color line is a guide to the eye. c) Pressure-dependent transient decay spectrum of $C_{24}H_{12}$.

continuously increased up to 5.0 GPa. The integrated intensity reached its maximum at 5.0 GPa, which was 2.07 times larger than at ambient pressure. At pressures 6.0–11.0 GPa, the emission intensity gradually decreased. A rapid decrease was observed at 12.0 GPa, which resulted in the abrupt reduction of ≈30% in the emission intensity, and the emission color changed from green to yellow and then to red. The emission intensity weakened continuously at pressures >12.0 GPa and disappeared at 23.0 GPa. When the pressure decreased from 23.6 GPa, the integrated intensity recovered, however, the CIE coordinates returned only to the green region (Figure S6, Supporting Information). Furthermore, when the pressure was decreased from 33.0 GPa in the second run, both the intensity and CIE coordinates were not recovered.

The observed spectrum at any pressure is the sum of a series of many energy transitions from various vibrational levels of the ground state to various levels of the excited state. The strength of each individual transition depends on the population at the excited state. Pressure initially alters the conformational distribution of molecules in the ground state, which in turn leads to significant spectral changes after excitation. The pressure-induced transition between different symmetry groups leads to large changes in the strength of the intermolecular interaction strength and thus to absorption and fluorescence. Therefore, the change in the shape of the emission band with increasing pressure indicates the changes in the electronic structure of coronene. It should be noted that the critical pressure points for the increase or decrease in the intensity were almost similar for the different measurements; however, their percentages varied, depending, for instance, on the thickness of the sample, or the position of the crystal surface measured. Both the redshifts and the changes in emission intensity were responsible for the change in the emission color that was observed in the PL micrographs.

To obtain more information on the PL property, we measured the transient decay spectrum at various pressures. Once the pressure was applied, the decay time of prompt and delayed fluorescence was suppressed. On the contrary, the relative amplitude of the delayed component increased significantly during compression up to 0.2 GPa. At pressures >1.2 GPa, the delayed component is suppressed continuously and only the prompt component was observed above 14.2 GPa. This result indicates that at least two mechanisms were involved in the pressure-induced emission enhancement (PIEE) of coronene. The emission enhancement at 0.2 GPa with the increased delayed component can be attributed to an enhancement of the TADF as energy gap between singlet and triplet states becomes smaller. Indeed, at 0.2 GPa, weight fraction of delayed component rapidly increased to 67%, which lead to an increase emission intensity by 30%. Above 1.2 GPa, the suppression of the delayed component could be attributed to the suppression of the TADF. The PIEE above 1.2 GPa can be attributed to the possible suppression of the non-radiative decay process, which played a key role in enhancing the emission efficiency.[24] Above 14.2 GPa, non-radiative decay channel dominates, causing a quenching of the emission intensity.[25] Further studies are required to clarify the mechanisms of the PIEE observed in coronene. The fit results obtained at each pressure are summarized in Table S4 (Supporting Information).

It is known that the mechanism of piezochromic phenomena is closely related to the electronic bandgap of luminescent materials. For semiconductors that exhibit bandgaps in the visible range, UV–vis absorption spectroscopy is a powerful technique for measuring the optical bandgap.[26] **Figure 4**a shows the in situ UV–vis absorption spectra. Upon compression, the absorbance increased rapidly and gradually broadened while the color of the crystals darkened (Figure S7, Supporting Information).

At higher pressures, the broadening and continuous red shifting of the UV–vis absorption spectra extended to longer

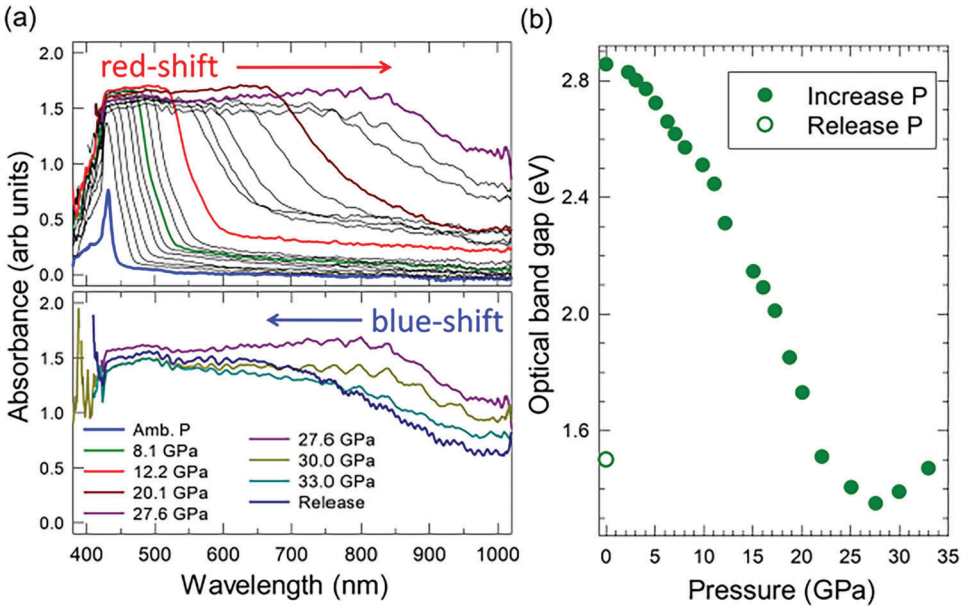

Figure 4. a) Pressure-dependent UV–vis absorption spectra of $C_{24}H_{12}$, showing red/blue shift below/above 27.6 GPa. b) Optical bandgap energy with respect to pressure.

wavelengths, eventually covering the entire visible and near infrared region. The total redshift during compression was 500 nm, with 18.1 nm/GPa. At pressures >28.0 GPa, a sudden change in the pressure dependence of the absorption edge was observed, and it migrated back to a shorter wavelength. Figure 4b shows the optical bandgap as a function of pressure.

The optical bandgap of coronene extracted from the UV–vis absorption systematically decreased from 2.85 eV at ambient conditions to 1.35 eV at 27.6 GPa, with a closure rate of −54 meV GPa^{-1}. Above 28 GPa, the bandgap re-opening emerged with the abrupt blue shift of absorption edge, the estimated bandgap was 1.47 eV at 33 GPa. The optical bandgap of 1.50 eV remained unchanged even when the pressure was completely released. In the second run, we collected UV–vis absorption spectra between 9.0 and 23.6 GPa, and decreased to 0.2 GPa, where we observed similar bandgap closure and complete recovery of the spectrum at ambient conditions. This demonstrates the excellent reversibility of the piezochromic behavior at pressures <24.0 GPa (Figure S8, Supporting Information). The re-opening of the optical bandgap coupled with the irreversibility of the spectroscopy suggests that molecule amorphization occurred at pressures >27.0 GPa.

To verify the effect of compression on intermolecular interactions, we performed an in situ high-pressure Raman spectroscopy experiment at RT up to 30 GPa. **Figure 5** shows the evolution of the lattice modes in the low-frequency Raman spectrum of coronene obtained using a 633 nm excitation laser. At 0.2 GPa, two lattice modes (L_1 and L_2), which were particularly sensitive to phase transitions, split into doublets producing a spectrum that was a fingerprint of the β-polymorph.[19,27] The polymorph change at 0.2 GPa, coincided with a sharp increase in the PL intensity observed at the same pressure. At 0.8 GPa, the L_{2a} peak split and formed another doublet, indicating a structural change. With further increase in pressure, no further drastic changes were observed in the Raman spectra up to 8.8 GPa, in which the Raman modes were significantly obscured by fluorescence. A broad and intense PL emission band at 7.4 GPa was observed in all the spectra acquired using the 785, 633, and 532 nm laser sources masking all Raman bands. When the pressure was reduced to 0.1 GPa, the γ-polymorph Raman modes were recovered (Figure 5b). Because the intensity of PL was significantly reduced at pressures >12.0 GPa, the Raman spectra were collected at various pressures up to 30 GPa during the second measurement (Figure S9, Supporting Information). By using a highly focused Raman system equipped with a 660 nm excitation laser, Raman modes at pressures up to 13.5 GPa were observed before being obscured by fluorescence. Subsequently, the obscured Raman modes became visible again at 19.0 GPa under red-shifted and reduced fluorescence. A well-patterned spectral profile was observed up to 26.0 GPa. A rapid broadening and disappearance of Raman modes were observed at pressures >27.0 GPa. The Raman modes of neither the γ- nor β-polymorph were recovered even after the pressure was completely released. The disappearance of the spectral features coupled with the irreversibility of the transition suggests that molecular amorphization occurred above 27.0 GPa.

To obtain missing vibrational information of coronene at pressures between 9 and 18 GPa, we performed a complementary IR spectroscopy under compression. At high pressure, IR is also a useful technique for identifying changes in molecular conformation as their vibrational modes are extremely sensitive to alternations of the molecular conformation but are not affected by redshift or fluorescence enhancement.[28] As shown in **Figure 6**, significant changes in the absorbance patterns of the C—H bending region (<1000 cm^{-1}) and C—H stretching region (2900–3100 cm^{-1}) were observed in response to increases in pressure >1.5 GPa. The IR vibrational bands exhibited splitting of peaks and appearance of new modes, whose intensity increased

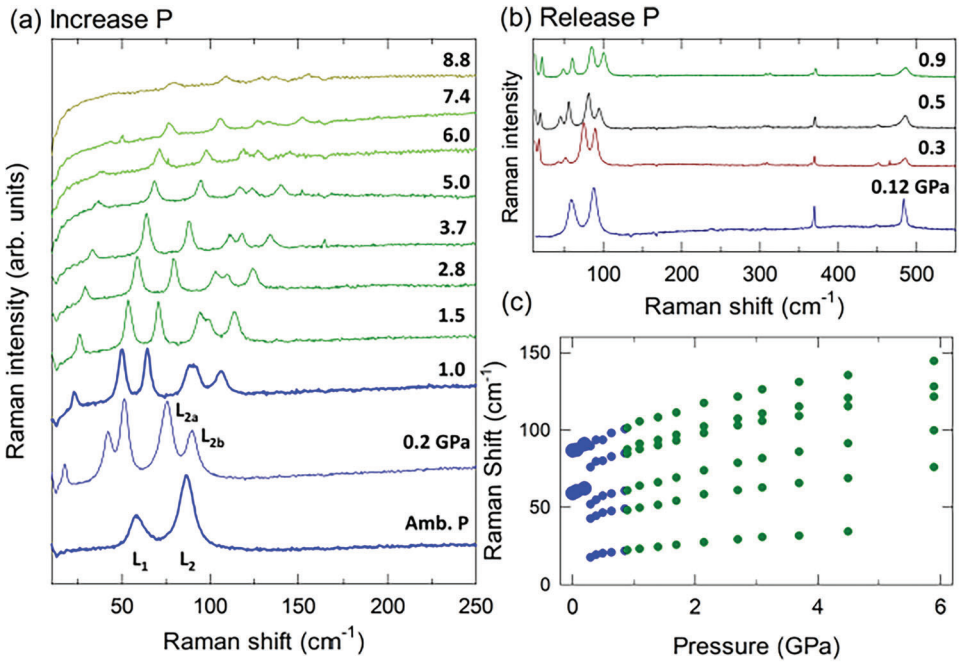

Figure 5. Selected Raman spectra of $C_{24}H_{12}$ at pressures <9 GPa obtained during a) pressure increased up to 9 GPa and b) pressure release from 9 GPa. c) Pressure dependence of Raman peak frequencies.

continuously with increasing pressure, reaching its maximum at 12.5 GPa. With further compression, the split IR peaks gradually began to merge, and at 18 GPa the intensity of the peak of the intramolecular C—H coupling vibration started to decrease. These changes in intensity, discontinuous shift, splitting, and appearance or disappearance of modes are indications of phase transition onset. At pressures >27.0 GPa, all IR peaks exhibited a rapid decrease in intensity. The original phase was not recovered upon decompression from 40.2 GPa, leaving broad humps in the C—H stretching region. The disappearance of IR spectral features and the irreversibility of this transition suggest that amorphization initiated at pressures above 27.0 GPa.

The IR spectrum of the recovered product was comparable to that of amorphous hydrogenated carbons obtained from pressurized benzene.[29] Some of the differences between them are caused by the residual coronene that did not undergo complete amorphization. It should be noted that the low-pressure spectral features were fully recovered when the pressure was released

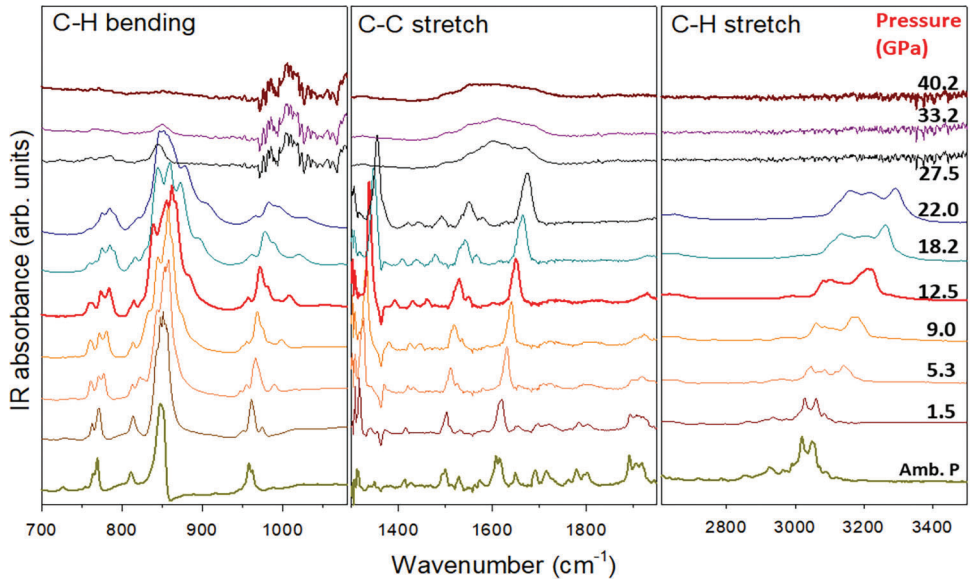

Figure 6. Selected pressure-dependent IR spectra of single-crystal $C_{24}H_{12}$ from ambient pressure up 40.2 GPa.

below 27.0 GPa (e.g., from 22.0 GPa) (Figure S4, Supporting Information), which was consistent with both UV–vis absorption and Raman spectroscopy measurements.

We performed an in situ high-pressure synchrotron PXRD experiment at RT to 22 GPa to better understand the relationship between structure and optical properties. Selected SPXRD profiles of coronene obtained at different pressures are shown in **Figure 7**.

The data shows that the reflection intensities were in good agreement with the single-crystal data at ambient pressure. Considering the cell parameters and space group extracted from the single-crystal data, the unit cell metrics of the polycrystalline data were evaluated at all pressures using the LeBail algorithm.

During compression, the PXRD diffraction profiles exhibited drastic changes at 1.0, 12.0, and 22.3 GPa, which agreed well with the changes observed in PL emission spectra and the phase transitions indicated by the Raman and IR spectroscopy measurements. At ambient conditions, coronene adopts a monoclinic γ-herringbone structure with space group $P2_1/n$, which underwent three phase transitions: Phase II-$P2/m$ (monoclinic), phase III-$Pmmm$ (orthorhombic) and Phase IV-$P2$(monoclinic). The transitions of Phases II and III agreed well with earlier reports[17]; however, the existence of Phase IV has not yet been reported (Figure S10, Supporting Information). The polymorph change to a β-herringbone motif observed at 0.2 GPa in Raman spectroscopy was not observed in PXRD measurements. That is, identification of polymorphs by X-ray analysis can be difficult, particularly when small energy changes result in different phases that occur in the same batch or even in the same crystallite.

We found that the optical properties of coronene depend largely on structural alternations. Blue emission was observed when coronene molecules were packed in either a γ-herringbone or β-herringbone assembly of monoclinic symmetry ($P2_1/n$ space group). Green emission was observed when coronene molecules were packed in a monoclinic arrangement ($P2/m$ space group). Red emission was observed when coronene molecules adopted an orthorhombic architecture ($Pmmm$ space group). PL emission disappeared during the structural transition to a monoclinic ($P2$) arrangement before the amorphization of coronene occurred at 27.0 GPa (Figure S11, Supporting Information). However, the determination of crystal structure accurately in organic molecular solids at high pressure is extremely challenging. Further investigation is required such as the single-crystal XRD to solve the crystal structure at high pressure.

We observed full-color piezochromic luminescence of coronene nano-rod at RT, which makes coronene a rare single-component material that can achieve RGB emission through simple modification of flexible crystallographic symmetry.

In addition, we found that coronene exhibited a novel PIEE phenomenon during compression up to 5.0 GPa, where a drastic emission enhancement was observed reaching 200% PL intensity compared to that at ambient conditions. This emission enhancement from blue to green agreed well with previous results reported by Zhang et al.[27] for coronene dissolved in two different solutions. They observed a blue emission from coronene in a THF solution and a four-time stronger green emission from coronene in an aqueous solution, caused by the aggregation of coronene molecules. To date, the mechanisms for PIEE in organic molecules have not been clarified. When organic molecules

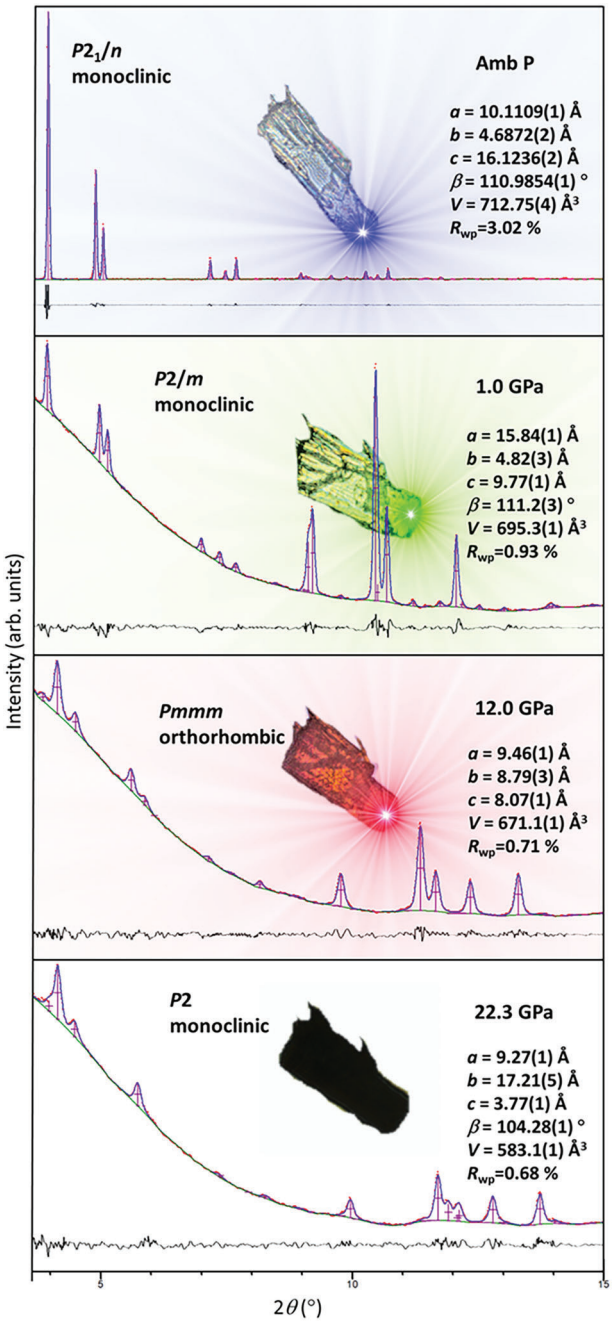

Figure 7. Final observed (red dots) and calculated (solid blue line) PXRD profile from Rietveld refinement using PXRD data of $C_{24}H_{12}$ at ambient pressure (top) and the results of peak intensity extraction from an indexed powder diffractogram using the Le-Bail algorithm (1.0, 12.0, and 22.3 GPa). The lower solid green lines indicate the fitted background contributions. The lower solid black lines indicate the difference profiles, whereas the pink and purple inner markers indicate the reflection positions at ambient and selected high pressures, respectively. Inset: optical image of $C_{24}H_{12}$ at each pressure: pale-yellow (Amb. P), yellow (1 GPa), dark-orange (12.0 GPa), and black (22.3 GPa).

absorb photons, each absorbed photon generates singlet excitons in the excited states that undergo various relaxation processes involving either non-radiative or radiative pathways. In pure organic molecules, most excitons relax to the ground state via a non-radiative pathway, often resulting in low luminescence efficiency. PIEE is attributed to the emission enhancement by inhibiting non-radiative energy dissipation, such as intramolecular rotations and vibrations. On the contrary, pressure-induced emission quenching occurred when the π-π stacking interactions between molecules were enhanced, resulting in non-radiative decay. Therefore, the competition between inhibition/induction of non-radiative decay is key, and it is largely modified by changes in molecular packing that can be directly observed using IR spectroscopy.[28] In the case of coronene, at pressures >1.5 GPa, an increase in the non-radiative vibration process was observed owing to the blue shift of the C—H stretching vibrational modes as pressure increased. Theoretically, this should lead to a decrease in the emission intensity. On the contrary, the C—H bending vibration modes exhibited peak splitting, broadening, and red-shifting resulting from the crystal structure transition at 1.5 GPa. As this trend continued, the PL emissions were enhanced and maintained their high intensity at pressures up to 12.5 GP. At pressures >12.5 GPa, the vibrational modes started to merge and blue-shift as a result of the phase transition, thereby attenuating the intensity of PL. This indicates that the non-radiative vibrational processes were suppressed at pressures above 1.5 GPa, causing an intense green emission. However, owing to the structural transition, this suppression mechanism disappeared, resulting in a weaker red emission. In contrast, the PIEE observed at 0.2 GPa, could be attributed to an enhancement of the delayed emission, which was evident from the increase in the delayed component in the PL decay measurement. The intensity of the delayed component of coronene could be enhanced either by suppressing the energy gap between the lowest excited triplet and singlet states of coronene,[29] or by suppressing the non-radiative recombination of excitons in STE.[30, 31] Additional studies are required to clarify the mechanisms of the PIEE observed in coronene. Nevertheless, at pressures above 1.2 GPa, the blue delayed emission disappeared as a result of the structural transition, leaving prompt green fluorescence emission.

3. Conclusion

In this study, we prepared single-crystalline coronene nano-rods that exhibit blue emission under UV light. We investigated the pressure evolution of their optical properties, structural evolution, and chemical stability at pressures up to 40 GPa through in situ high-pressure experiments. We found that coronene nanorods are rare examples of small molecule single-component systems that exhibit full-color piezochromic luminescence at RT. We confirmed that the emission color changes were strictly related to the flexible crystallographic symmetry of coronene. Our study can provide a valuable understanding of the pressure-dependent structure-to-property relationship of single crystalline coronene and offer a high motivation for the preparation of coronene single crystals with different crystal structures that exhibit RGB emission at ambient conditions. Single-component materials with these optical properties, which can be prepared without complex and costly organic synthetic procedures can be important for application in various optoelectronic materials.

4. Experimental Section

Sample Preparation: Coronene ($C_{24}H_{12}$) was purchased from TCI Chemicals ($C_{24}H_{12}$ >98%). Coronene single crystals were grown using a re-crystallization technique, in which coronene powder was dissolved in 50 mL of anhydrous tetrahydrofuran (THF) and heated to 320 K on a magnetic plate with continuous stirring. Fifty milliliters of anhydrous hexane was slowly added to form a layer on the solution. The obtained re-crystallized single-crystal coronene was washed with ethanol.

Optical Spectroscopy: UV–vis absorption and PL spectroscopy measurements were conducted using an integrated micro-region spectroscopy system Gora-UVN-FL (Ideaoptics, Shanghai). A single-crystal of coronene ($100 \times 30 \times 10\ \mu m^3$), with a ruby ball, was loaded into a sample chamber, and silicone oil was used as a pressure transmitting medium. The pressure was determined by the fitting pressure shift of the ruby fluorescence line below 20 GPa. The diamond fluorescence line was used above 20 GPa. UV–vis absorption spectra were collected using a Xenon light source ranging between 300 and 1100 nm. PL spectra were obtained using a 405 nm excitation laser, integrated over 1000 µs, with power maintained below 1.1 mW to avoid irradiation damage to the sample.

Supporting Information

Supporting Information is available from the Wiley Online Library or from the author.

Acknowledgements

This study was financially supported by the National Key Research and Development Program of China (2018YFA0305703 and 2022YFA1402301) and the National Natural Science Foundation of China (NSFC: U1930401 and 11874075).

Conflict of Interest

The authors declare no conflict of interest.

Data Availability Statement

The data that support the findings of this study are available in the Supporting Information. The CCDC number of the coronene, $C_{24}H_{12}$ crystal (2141417).

Keywords

full-color luminescence, polycyclic aromatic hydrocarbons, pressure-induced emission enhancement, RGB emission, structure transition

Received: March 9, 2023
Revised: July 6, 2023
Published online:

[1] K. Jiang, S. Sun, L. Zhang, Y. Lu, A. Wu, C. Cai, H. Lin, *Angew. Chem., Int. Ed.* **2015**, *54*, 5360.

[2] H. Uoyama, K. Goushi, K. Shizu, H. Nomura, C. Adachi, *Nature* **2012**, *492*, 234.
[3] H. Seiler, M. Krynski, D. Zahn, S. Hammer, Y. W. Windsor, T. Vasileiadis, J. Pflaum, R. Ernstorfer, M. Rossi, H. Schwoerer, *Sci. Adv.* **2021**, *7*, eabg0869.
[4] Y. Yang, M. Lowry, C. M. Schowalter, S. O. Fakayode, J. O. Escobedo, X. Xu, H. Zhang, T. J. Jensen, F. R. Fronczek, I. M. Warner, R. M. Strongin, *J. Am. Chem. Soc.* **2006**, *128*, 14081.
[5] A. Wakamiya, K. Mori, S. Yamaguchi, *Angew Chem Int Ed Engl* **2007**, *46*, 4273.
[6] C. Yuan, S. Saito, C. Camacho, S. Irle, I. Hisaki, S. Yamaguchi, *J. Am. Chem. Soc.* **2013**, *135*, 8842.
[7] S. Tong, J. Dai, J. Sun, Y. Liu, X. Ma, Z. Liu, T. Ma, J. Tan, Z. Yao, S. Wang, H. Zheng, K. Wang, F. Hong, X. Yu, C. Gao, X. Gu, *Nat. Commun.* **2022**, *13*, 5234.
[8] a) S. Ito, *Chem. Lett.* **2021**, *50*, 649; b) A. Li, S. Xu, C. Bi, Y. Geng, H. Cui, W. Xu, *Mater. Chem. Front.* **2021**, *5*, 2588; c) N. C. Harms, H. Kim, A. J. Clune, K. A. Smith, K. R. O'Neal, A. V. Haglund, D. G. Mandrus, Z. Liu, K. Haule, D. Vanderbilt, J. L. Musfeldt, *npj Quantum Mater.* **2020**, *5*, 56; d) Y. Fang, L. Zhang, L. Wu, J. Yan, Y. Lin, K. Wang, W. L. Mao, B. Zou, *Angew. Chem. Int. Ed.* **2019**, *58*, 15249.
[9] a) H. Ran, Z. Zhao, X. Duan, F. Xie, R. Han, H. Sun, J. Hu, *J. Mater. Chem. C* **2021**, *9*, 260; b) A. Seeboth, D. Loetzsch, R. Ruhmann, *Am. J. Mater. Sci.* **2012**, *1*, 139; c) L. Liu, K. Wang, J. Deng, Z. Zhang, Y. Wang, Y. Ma, *Faraday Discuss.* **2017**, *196*, 415; d) W. E. Lee, C. L. Lee, T. Sakaguchi, M. Fujiki, G. Kwak, *Chem. Commun.* **2011**, *47*, 3526.
[10] a) J. Y. Hu, Y. J. Pu, G. Nakata, S. Kawata, H. Sasabe, J. Kido, *Chem. Commun.* **2012**, *48*, 8434; b) E. Venuti, R. G. Della Valle, L. Farina, A. Brillante, M. Masino, A. Girlando, *Phys. Rev. B* **2004**, *70*, 104106; c) S. Fanetti, M. Citroni, L. Malavasi, G. A. Artioli, P. Postorino, R. Bini, *J. Phys. Chem. C* **2013**, *117*, 5343.
[11] G. R. Desiraju, A. Gavezzotti, *Acta Crystallogr., Sect. B: Struct. Sci., Cryst. Eng. Mater.* **1989**, *45*, 473.
[12] a) U. Rohr, P. Schlichting, A. Böhm, M. Gross, K. Meerholz, C. Bräuchle, K. Müllen, *Angew. Chem.* **1998**, *110*, 1463; b) Z. An, J. Yu, B. Domercq, S. C. Jones, S. Barlow, B. Kippelen, S. R. Marder, *J. Mater. Chem.* **2009**, *19*, 6688.
[13] D. Wu, H. Zhang, J. Liang, H. Ge, C. Chi, J. Wu, S. H. Liu, J. Yin, *J. Org. Chem.* **2012**, *77*, 11319.
[14] a) Y. Dai, H. Liu, T. Geng, F. Ke, S. Niu, K. Wang, Y. Qi, B. Zou, B. Yang, W. L. Mao, Y. Lin, *J. Mater. Chem. C* **2021**, *9*, 934; b) Y. Dong, B. Xu, J. Zhang, X. Tan, L. Wang, J. Chen, H. Lv, S. Wen, B. Li, L. Ye, B. Zou, W. Tian, *Angew Chem Int Ed Engl* **2012**, *51*, 10782; c) H. Liu, Y. Gu, Y. Dai, K. Wang, S. Zhang, G. Chen, B. Zou, B. Yang, *J. Am. Chem. Soc.* **2020**, *142*, 1153; d) H. Liu, Y. Dai, Y. Gao, H. Gao, L. Yao, S. Zhang, Z. Xie, K. Wang, B. Zou, B. Yang, Y. Ma, *Adv. Opt. Mater.* **2018**, *6*, 1800085; e) T. Schillmöller, R. Herbst-Irmer, D. Stalke, *Adv. Opt. Mater.* **2021**, *9*, 2001814; f) H. Liu, Y. Shen, Y. Yan, C. Zhou, S. Zhang, B. Li, L. Ye, B. Yang, *Adv. Funct. Mater.* **2019**, *29*, 1901895.
[15] J. M. Robertson, J. G. White, *Nature* **1944**, *154*, 605.
[16] J. Potticary, L. R. Terry, C. Bell, A. N. Papanikolopoulos, P. C. M. Christianen, H. Engelkamp, A. M. Collins, C. Fontanesi, G. Kociok-Köhn, S. Crampin, E. Da Como, S. R. Hall, *Nat. Commun.* **2016**, *7*, 11555.
[17] a) E. Jennings, W. Montgomery, P.h. Lerch, *J. Phys. Chem. B* **2010**, *114*, 15753; b) X. M. Zhao, J. Zhang, A. Berlie, Z. X. Qin, Q. W. Huang, S. Jiang, J. B. Zhang, L. Y. Tang, J. Liu, C. Zhang, G. H. Zhong, H. Q. Lin, X. J. Chen, *J. Chem. Phys.* **2013**, *139*, 144308; c) A. D. Chanyshev, A. Y. Likhacheva, P. N. Gavryushkin, K. D. Litasov, *J. Struct. Chem.* **2016**, *57*, 1489.
[18] T. Yamamoto, S. Nakatani, T. Nakamura, K. Mizuno, A. H. Matsui, Y. Akahama, H. Kawamura, *Chem. Phys.* **1994**, *184*, 247.
[19] T. Salzillo, A. Giunchi, M. Masino, N. Bedoya-Martínez, R. G. Della Valle, A. Brillante, A. Girlando, E. Venuti, *Cryst. Growth Des.* **2018**, *18*, 4869.
[20] A. H. Matsui, K. Mizuno, *J. Phys. D: Appl. Phys.* **1993**, *26*, B242.
[21] a) P. Kubelka, F. A. Munk, *Tech. Phys.* **1931**, *12*, 593; b) Y. Kondo, K. Yoshiura, S. Kitera, H. Nishi, S. Oda, H. Gotoh, Y. Sasada, M. Yanai, T. Hatakeyama, *Nat. Photonics* **2019**, *13*, 678.
[22] P. Makuła, M. Pacia, W. Macyk, *J. Phys. Chem. Lett.* **2018**, *9*, 6814.
[23] J. L. Kropp, W. R. Dawson, *J. Phys. Chem.* **1967**, *71*, 4499.
[24] a) Y. Gu, K. Wang, Y. Dai, G. Xiao, Y. Ma, Y. Qiao, B. Zou, *J. Phys. Chem. Lett.* **2017**, *8*, 4191; b) J. Ochi, K. Tanaka, Y. Chujo, *Angew. Chem. Int. Ed.* **2023**, *62*, e202214397; c) Y. Fang, L. Zhang, Y. Yu, X. Yang, K. Wang, B. Zou, *CCS. Chem.* **2021**, *2*, 2203.
[25] Y. Fang, J. Wang, L. Zhang, G. Niu, L. Sui, G. Wu, K. Yuan, K. Wang, B. Zou, *Chem. Sci.* **2023**, *14*, 2652.
[26] J. C. S. Costa, R. J. S. Taveira, C. F. R. A. C. Lima, A. Mendes, L. M. N. B. F. Santos, *Opt. Mater.* **2016**, *58*, 51.
[27] N. Bannister, J. Skelton, G. Kociok-Köhn, T. Batten, E. D. Como, S. Crampin, *Phys. Rev. Mater.* **2019**, *3*, 125601.
[28] E. O'Bannon, Q. Williams, *Phys. Chem. Miner.* **2016**, *43*, 181.
[29] a) L. Ciabini, M. Santoro, F. A. Gorelli, R. Bini, V. Schettino, S. Raugei, *Nat. Mater.* **2007**, *6*, 39; b) L. Ciabini, M. Santoro, R. Bini, V. Schettino, *J. Chem. Phys.* **2002**, *116*, 2928.
[30] J. Xiao, H. Yang, Z. Yin, J. Guo, F. Boey, H. Zhang, Q. Zhang, *J. Mater. Chem.* **2011**, *21*, 1423.
[31] Q. Li, Z. Chen, B. Yang, L. Tan, B. Xu, J. Han, Y. Zhao, J. Tang, Z. Quan, *J. Am. Chem. Soc.* **2020**, *142*, 1786.